Energy and radiative properties of the $(3)^1\Pi$ and $(5)^1\Sigma^+$ states of RbCs: Experiment and theory

K. Alps, A. Kruzins, O. Nikolayeva, M. Tamanis, and R. Ferber*
Laser Center, University of Latvia, 19 Rainis Boulevard, Riga LV-1586, Latvia

E. A. Pazyuk and A. V. Stolyarov†
Department of Chemistry, Lomonosov Moscow State University, 119991 Moscow, Leninskie gory 1/3, Russia
(Received 15 June 2017; published 11 August 2017)

We combined high-resolution Fourier-transform spectroscopy and large-scale electronic structure calculation to study energy and radiative properties of the high-lying $(3)^1\Pi$ and $(5)^1\Sigma^+$ states of the RbCs molecule. The laser-induced $(5)^1\Sigma^+$,$(4)^1\Sigma^+$,$(3)^1\Pi \rightarrow A(2)^1\Sigma^+ \sim b(1)^3\Pi$ fluorescence (LIF) spectra were recorded by the Bruker IFS-125(HR) spectrometer in the frequency range $\nu \in [5500, 10\,000]$ cm^{-1} with the instrumental resolution of 0.03 cm^{-1}. The rotational assignment of the observed LIF progressions, which exhibit irregular vibrational-rotational spacing due to strong spin-orbit interaction between $A^1\Sigma^+$ and $b^3\Pi$ states was based on the coincidences between observed and calculated energy differences. The required rovibronic term values of the strongly perturbed $A \sim b$ complex have been calculated by a coupled-channels approach for both ^{85}Rb^{133}Cs and ^{87}Rb^{133}Cs isotopologs with accuracy of about 0.01 cm^{-1}, as demonstrated in A. Kruzins *et al.* [J. Chem. Phys. **141**, 184309 (2014)]. The experimental energies of the upper $(3)^1\Pi$ and $(5)^1\Sigma^+$ states were involved in a direct-potential-fit analysis performed in the framework of inverted perturbation approach. Quasirelativistic *ab initio* calculations of the spin-allowed $(3)^1\Pi$,$(5)^1\Sigma^+ \rightarrow$ (1-4)$^1\Sigma^+$,(1-3)$^1\Pi$ transition dipole moments were performed. Radiative lifetimes and vibronic branching ratios of radiative transitions from the $(3)^1\Pi$ and $(5)^1\Sigma^+$ states were evaluated. To elucidate the origin of the Λ-doubling effect in the $(3)^1\Pi$ state, the angular coupling $(3)^1\Pi$-$(1\text{-}5)^1\Sigma^+$ electronic matrix elements were calculated and applied for the relevant q-factors estimate. The intensity distributions simulated for the particular $(5)^1\Sigma^+$;$(3)^1\Pi \rightarrow A \sim b$ LIF progressions have been found to be remarkably close to their experimental counterparts.

DOI: 10.1103/PhysRevA.96.022510

I. INTRODUCTION

Accurate knowledge of energy and radiative properties of a high-lying excited state of heavy polar alkali-metal diatomic molecules is important for selecting the efficient optical routes for accessing so-called intermediate electronic states of the mixed singlet-triplet nature in one- or two-photon transitions [1,2]; besides, it provides an unambiguous test of the reliability of state-of-the-art *ab initio* electronic structure calculations [3].

In particular, the RbCs molecule has been actively studied both theoretically and experimentally because of its successful employment for obtaining ultracold polar molecular species [4–8]. At the same time, the accurate empirical information on the higher electronic states of RbCs is still very scarce. To our best knowledge, the only electronic state approaching the atomic limit higher than 5^2P(Rb) + 6^2S(Cs), which was studied experimentally with high resolution in a broad-enough range of vibrational v' and rotational J' levels, is the $(4)^1\Sigma^+$ state [9,10] (see Fig. 1); this state appeared to be promising for two-step optical cycles to achieve ultracold RbCs in the absolute ($v_X = 0$, $J_X = 0$) ground state because of efficient transitions to the lowest electronic $X^1\Sigma^+$ and $a^3\Sigma^+$ states.

The information on other high-lying states of RbCs is fragmentary, since the main goal often was to use the subsequent laser-induced fluorescence (LIF) to study the ground $X^1\Sigma^+$ state. For instance, molecular constants (Dunham coefficients) and corresponding Rydberg-Klein-Rees (RKR) potentials for $(2,4,5)^1\Pi$ and $(3,7)^1\Sigma^+$ states of RbCs have been obtained [11] by the Fourier transform spectroscopy (FTS) method in the energy regions 20 000–22 000 cm^{-1} and 13 000–15 000 cm^{-1}. As far as high-resolution FTS of LIF from high-lying electronic states to the ground state is concerned, the main difficulties are often connected with the low probability of optical transitions due to a small transition electric dipole moment. In many cases, even if a low probability transition may still be used to excite a high-lying state, it is hopeless to convincingly detect dispersed LIF backwards to the ground $X^1\Sigma^+$ state. Therefore, the alternative methods might be preferable, such as polarization labeling spectroscopy, two-photon optical transitions, or multiphoton ionization. Information on the $(4)^1\Sigma^+$, $(3)^1\Pi$, $(5)^1\Sigma^+$, $(6)^1\Sigma^+$, $(1)^3\Delta$, and $(4)^3\Pi$ states obtained from the high-resolution resonance-enhanced two-photon ionization (RE2PI) spectroscopy of RbCs in a molecular beam is contained in Refs. [12–15]; the spectroscopic data on $(5)^1\Sigma^+$ and $(3)^3\Pi$ states can be found in Ref. [14].

In the present study, we suggest an alternative method to overcome weak LIF to the ground state: to replace the latter by the first excited state, namely by the LIF transitions to the strongly mixed $A(2)^1\Sigma^+ \sim b(1)^3\Pi$ system (see Fig. 1). This opportunity has been made feasible by the recent high-accuracy deperturbation analysis of the RbCs $A \sim b$ complex [16], which allows one to reproduce the required rovibronic term values of the complex with the accuracy quite comparable with that of the ground state. We focused our study on the $(3)^1\Pi$ and $(5)^1\Sigma^+$ states of RbCs with the purpose to obtain more detailed energy information needed to perform the direct-potential-fit (DPF) analysis of these states. We also performed

*ferber@latnet.lv
†avstol@phys.chem.msu.ru

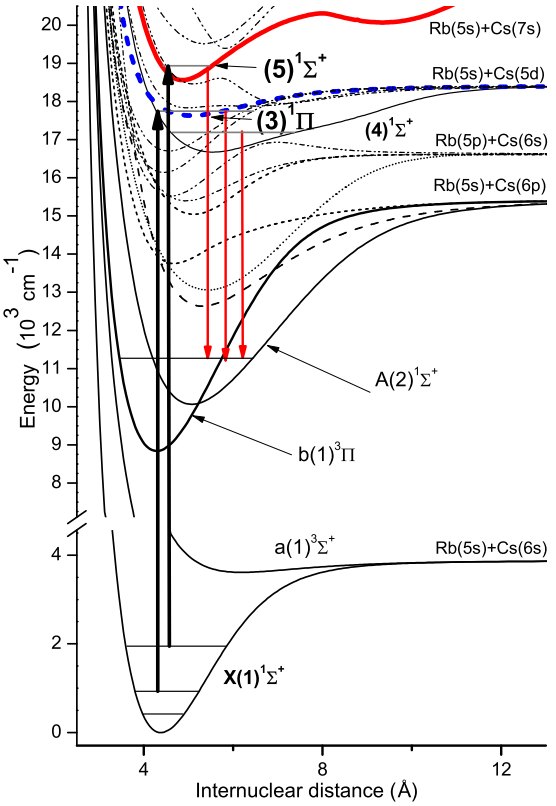

FIG. 1. Scheme of the lowest electronic terms of RbCs molecule [17]. Vertical arrows mark excitation-observation transitions in the present FTS LIF experiment.

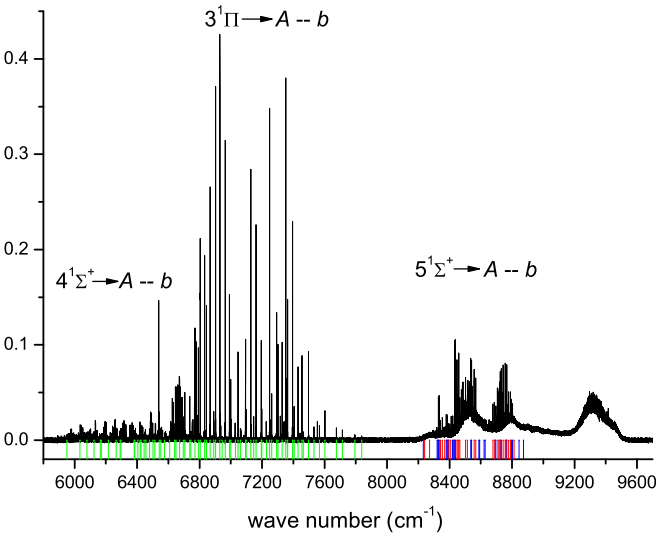

FIG. 2. Example of FTS LIF spectrum to the $A \sim b$ complex recorded at excitation laser frequency 17 672.697 cm^{-1} using long-pass edge filter 1050 nm. Green bars mark the singlet Q transitions from the $(3)^1\Pi$ level corresponding to $v' = 14$, $J' = 73$, and $E' =$ 17 787.008 cm^{-1}; red and blue bars mark the doublet P/R transitions from the $(5)^1\Sigma^+$ levels with $v' = 5$, $J' = 211$, $E' = 19\,346.149$ cm^{-1} and $v' = 7$, $J' = 97$, $E' = 18\,974.387$ cm^{-1}, respectively.

ab initio calculations of potential energy curves (PECs) and transition dipole moments to estimate radiative properties of both states under study.

II. EXPERIMENT

In the experiment RbCs molecules were produced in the heat-pipe oven, which was loaded with 10g Cs and 5g Rb (natural mixture of isotopes) metals. Working temperature was 310 °C. For excitation the single mode ring dye laser Coherent 699-21 with Rhodamine 6G dye was used. Laser beam was sent into the heat-pipe and backward LIF spectra to the strongly mixed $A^1\Sigma^+$ and $b^3\Pi$ states from the upper $(3)^1\Pi$ and $(5)^1\Sigma^+$ states, as well as from accidentally excited $(4)^1\Sigma^+$ state, see Fig. 1, were recorded with the instrumental resolution of 0.03 cm^{-1} by means of FT spectrometer Bruker IFS-125(HR). LIF was detected in the range from 5500 to 10 000 cm^{-1} using an InGaAs detector. Laser frequency was selected within the range 16 700–17 800 cm^{-1}. This frequency range is very suitable to excite the $(4)^1\Sigma^+$ state, which typically gives rise to a strong $(4)^1\Sigma^+ \rightarrow A \sim b$ fluorescence [16]. Fortunately, the $(3)^1\Pi \rightarrow A \sim b$ system is partially shifted from the $(4)^1\Sigma^+ \rightarrow A \sim b$ system due to a different equilibrium internuclear distance of the upper state PECs. Thus, by monitoring in the expected range the $(3)^1\Pi \rightarrow A \sim b$ LIF signal in real time by means of FT spectrometer's Preview Mode at low resolution, it was possible to set the laser frequency in resonance with the $(3)^1\Pi(v', J') \leftarrow X^1\Sigma^+(v'', J'')$ transitions. An example of the recorded spectrum is shown in Fig. 2. In this particular case, an accidentally excited $(4)^1\Sigma^+ \rightarrow A \sim b$ system is strongly diminished when compared with the strongest part of the $(3)^1\Pi \rightarrow A \sim b$ system in the range 6800–7600 cm^{-1}. The LIF $(5)^1\Sigma^+ \rightarrow A \sim b$ is observed in the range 8400–8800 cm^{-1} and is typically weaker than the $(3)^1\Pi \rightarrow A \sim b$ system, at least for two reasons. First, as one can see in Fig. 1 the $(5)^1\Sigma^+$ state lies about 1500 cm^{-1} higher than the $(3)^1\Pi$ state; hence, the absorption transitions start from high, less-populated vibrational v'' levels of the ground state. Another reason is the continuum fluorescence observed in the range 8400–9600 cm^{-1}, which is overlapping with the $(5)^1\Sigma^+ \rightarrow A \sim b$ LIF. Since in the Preview Mode the continuum LIF is dominating, it was practically impossible to set the laser frequency in resonance to excite the $(5)^1\Sigma^+$ state. Nevertheless, we have managed to record more than 100 LIF progressions from the $(3)^1\Pi$ and also the $(5)^1\Sigma^+$ states to the $A \sim b$ complex, which exhibited an irregular wibrational-rotational spacing.

III. ROTATIONAL ASSIGNMENT OF THE IRREGULAR LIF PROGRESSIONS TO THE $A \sim b$ COMPLEX

Assignment of the observed $(5)^1\Sigma^+$, $(3)^1\Pi \rightarrow A^1\Sigma^+ \sim b^3\Pi$ transitions was based on the high-accuracy description of the $A \sim b$ complex [16], which ensures that its rovibronic term values can be reproduced with accuracy typically better than 0.01 cm^{-1} in a wide energy range.

The required rovibronic energy $E_{A\sim b}$ and relevant nonadiabatic vibrational wave function $\Phi_{A\sim b}$ of the $A \sim b$ complex were generated in advance for both ^{85}Rb^{133}Cs and ^{87}Rb^{133}Cs isotopologs by the numerical solution of the coupled-channels

(CC) radial equations [18]:

$$\left[-\mathbf{I}\frac{\hbar^2 d^2}{2\mu dR^2} + \mathbf{V}(R;\mu,J'') - \mathbf{I}E_{A\sim b}\right]\Phi_{\mathbf{A}\sim\mathbf{b}}(R) = 0, \quad (1)$$

where $\mathbf{I}$ is the identity matrix and μ is the reduced mass and the 4×4 symmetric matrix ($i \in [A^1\Sigma^+, b^3\Pi_{\Omega=0,1,2}]$) of the potential energy $\mathbf{V}(R;\mu,J'')$ consists of nonzero diagonal

$$\begin{aligned} V_{^1\Sigma^+} &= U_A + B[X+2] \\ V_{^3\Pi_0} &= U_{b0} + B[X+2] \\ V_{^3\Pi_1} &= U_{b0} + A_{01} + B[X+2] \\ V_{^3\Pi_2} &= U_{b0} + 2A_{so} + B[X-2] \end{aligned} \quad (2)$$

and off-diagonal

$$\begin{aligned} V_{^1\Sigma^+ - ^3\Pi_0} &= -\sqrt{2}\xi_{Ab0} \\ V_{^3\Pi_0 - ^3\Pi_1} &= -B\sqrt{2X} \\ V_{^3\Pi_1 - ^3\Pi_2} &= -B\sqrt{2(X-2)} \end{aligned} \quad (3)$$

matrix elements with

$$B = \frac{\hbar^2}{2\mu R^2}; \quad X \equiv J''(J''+1). \quad (4)$$

The rotationless $U_A(R)$ and $U_{b0}(R)$ PECs of the mutually perturbed singlet and triplet states as well as the corresponding spin-orbit coupling $\xi_{Ab0}(R)$ and the nonequidistant SO splitting $A_{01}(R) \neq A_{so}(R)$ functions were borrowed from Ref. [16]. The resulting term values data set of the $A\sim b$ complex is provided in the Supplemental Material [19].

The rotational assignment of the lines belonging to a particular LIF progression was performed in automatic regime with help of a homemade program, which searched for the coincidences between calculated and observed rovibrational differences. Two criteria served as a test of the correctness of the assignment. First, the assigned transitions belonging to a particular progression should yield to a coinciding, within a given accuracy, upper state energy. Second, the excitation laser frequency should be in resonance, within Doppler broadening, with some calculated absorption transition from the ground-state level. Moreover, all $(4)^1\Sigma^+ \rightarrow A\sim b$ transitions observed in the recorded LIF spectra were assigned, too, and the obtained $(4)^1\Sigma^+$ state term values were compared with the ones calculated by the empirical PEC from Ref. [10]. These tests unambiguously proved the reliability of the assigned procedure.

IV. DPF ANALYSIS

The present experimental term values of the $(3)^1\Pi$ and $(5)^1\Sigma^+$ states were incorporated, together with the preceding experimental data [13,14], in the DPF analysis performed in the framework of inverted perturbation approach (IPA) [20]. The adjusted adiabatic potentials $U_i^{\rm IPA}(R)$ of both studied states were defined in the pointwise interpolated by the natural cubic splines on a finite interval of internuclear distance R. The required initial points were extracted from the corresponding "difference-based" potentials $U_i^{\rm db}(R)$ constructed by Eq. (7) as described in Sec. V.

In order to take into account the Λ-doubling effect in the $(3)^1\Pi$ state explicitly, the conventional effective (rotational) potential used in the iteration solution of the radial Schrödinger equation was modified as

$$U^{J'} = U^{\rm IPA} + (1+sBQ)B[J'(J'+1)-1], \quad (5)$$

where $B(R)$ is given by Eq. (4) while $Q(R)$ is the *ab initio* precomputed function of the internuclear distance:

$$Q(R) = 2\sum_{^1\Sigma^+}\frac{\left|L^{\rm ab}_{^1\Pi - ^1\Sigma^+}\right|^2}{U^{\rm ab}_{^1\Pi} - U^{\rm ab}_{^1\Sigma^+}}. \quad (6)$$

The required potentials $U_i^{\rm ab}(R)$ and L-uncoupling electronic matrix elements $L_{ij}^{\rm ab}(R)$ between the $(3)^1\Pi$ and $(1\text{-}5)^1\Sigma^+$ states were obtained during the electronic structure calculation described in Sec. V. The scaling parameter s in Eq. (5) apparently vanishes for the f component of the $(3)^1\Pi$ state, whereas for the e component s is considered as the adjustable fitting parameter, which should be close to 1.

V. ELECTRONIC STRUCTURE CALCULATION

The adiabatic PECs $U_i^{\rm ab}(R)$ for the $i \in (1\text{-}5)^1\Sigma^+$, $(1\text{-}4)^1\Pi$ states, along with a spin-allowed $^1\Sigma^+ - ^1\Sigma^+$ and $^1\Pi - ^1\Sigma^+$ transition dipole moments $d_{ij}^{\rm ab}(R)$, were calculated in the basis of spin-averaged electronic wave functions corresponding to pure (a) Hund's coupling case. To elucidate an origin of the Λ-doubling effect observed in the $(3)^1\Pi$ state, the relevant angular coupling electronic matrix elements $L_{ij}^{\rm ab}(R)$ between the $(3)^1\Pi$ state and $(1\text{-}5)^1\Sigma^+$ states were evaluated as well. All calculations were performed in the wide range of internuclear distance $R \in [2.5,25]$ Å by means of the MOLPRO program [21].

Assuming that the originally calculated electronic energy weakly depends on the excitation energy, the R-dependent part of a systematic error in the original *ab initio* curves $U_i^{\rm ab}(R)$ was decreased for the excited states by means of a semiempirical expression [22]:

$$U_i^{\rm db} = \left[U_i^{\rm ab} - U_X^{\rm ab}\right] + U_X^{\rm emp}, \quad (7)$$

where $U_X^{\rm emp}(R)$ is the highly accurate empirical PEC available for the ground $X^1\Sigma^+$ state [23] of RbCs in a wide R range. Thus, the basis set superposition error (BSSE) is partly accounted for. The tabulated $U_i^{\rm ab}(R)$, $U_i^{\rm db}(R)$, $d_{ij}^{\rm ab}(R)$, and $L_{ij}^{\rm ab}(R)$ functions could be found in the ASCII format in the Supplemental Material [19].

The details of the computational procedure can be found elsewhere [24]. Briefly, the inner core shell of both rubidium and cesium atoms was replaced by the shape-consistent nonempirical effective core potentials [25] (ECP), leaving nine outer shells (eight subvalence plus one valence) electrons for explicit treatment (the basis set employed in the calculations is given in the Supplemental Material [19]). The optimized molecular orbitals were constructed from the solutions of the state-averaged complete active space self-consistent field (SA-CASSCF) problem for all 18 electrons on the lowest $(1\text{-}10)^1\Sigma^+$ and $(1\text{-}5)^1\Pi$ electronic states taken with equal weights [26]. The dynamical correlation was introduced by the internally contracted multireference configuration interaction (MR-CI) method [27], which was applied for only two

TABLE I. The static polarizability α_c [30] and cut-off radii r_c used for the core-polarization potentials of the Rb and Cs atoms. All parameters in a.u.

	α_c	r_c
Rb	9.096	0.389
Cs	15.687	0.243

valence electrons keeping the 16 subvalence electrons frozen. The core-polarization potentials [28] (CPPs) of both atoms were implemented in order to take into account for the pronounced core-valence correlation effects. The CPP cut-off radii (see Table I) were adjusted to reproduce experimental nonrelativistic energies [29] of the lowest excited Rb(5^2P) and Cs(5^2D) states, respectively.

VI. RESULTS AND DISCUSSION

A. Experimental term values and potential energy curves of the $(3)^1\Pi$ and $(5)^1\Sigma^+$ states

Overall, 493 rovibronic term values of the $(3)^1\Pi$ state and 292 term values of the $(5)^1\Sigma^+$ state were obtained in the present experiment. We expect that an uncertainty of measured term values is about 0.01–0.015 cm^{-1}; dominant contributions are the Doppler broadening of excitation transitions and the uncertainty of the calculated term values of the $A \sim b$ complex. Figures 3 and 4 show all experimental data set available for the $(3)^1\Pi$ and $(5)^1\Sigma^+$ states of both $^{85}Rb^{133}Cs$ and $^{87}Rb^{133}Cs$ isotopologs. Besides the present data set for the $(3)^1\Pi$ state, we incorporated in the DPF analysis 29 rotationless ($J' = 1$) term values from Ref. [13] for $v' \in [2,17]$ and $v' \in [3,17]$ vibrational levels of $^{85}Rb^{133}Cs$ and $^{87}Rb^{133}Cs$, respectively. For the $(5)^1\Sigma^+$ state, the originally measured absorption $(5)^1\Sigma^+ \leftarrow X\ ^1\Sigma^+$ line positions given in the

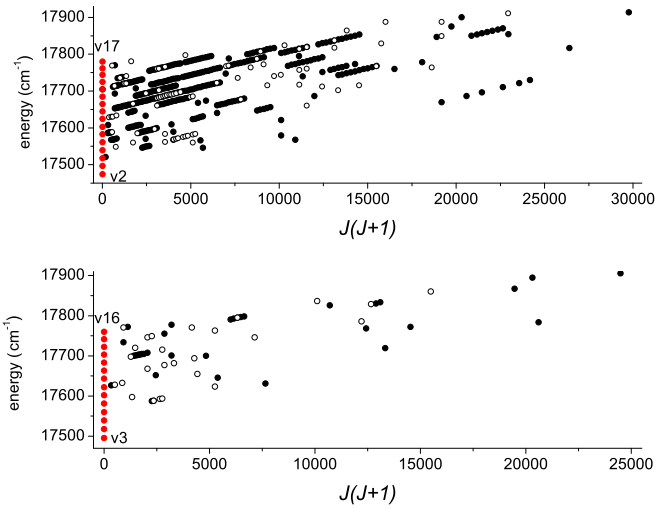

FIG. 3. Experimental term values data field available for the $(3)^1\Pi$ state: upper layer, $^{85}Rb^{133}Cs$; lower layer, $^{87}Rb^{133}Cs$. Empty circles denote e-symmetry levels; full circles denote f-symmetry levels. Red dots denote values extrapolated in Ref. [13] to the lowest $J' = 1$ levels.

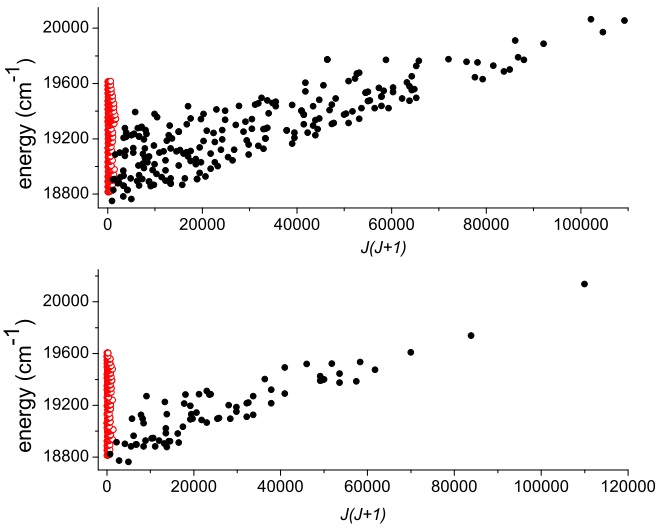

FIG. 4. Experimental term values data field available for the $(5)^1\Sigma^+$ state: upper layer, $^{85}Rb^{133}Cs$; lower layer, $^{87}Rb^{133}Cs$. Full circles denote the present experiment; red circles denote the low J'-value levels observed in Ref. [14].

EPAPS of Ref. [14] were added to the corresponding energy of the ground state calculated with the highly accurate empirical $U_X^{emp}(R)$ PEC [23]. Thus obtained 1196 rovibronic term values of both isotoplogs with $v' \in [6,31]$ and $J' \in [1,41]$ were involved into the DPF analysis along with the present $(5)^1\Sigma^+$ data. The data from Ref. [13] for the $(3)^1\Pi$ state and from Ref. [14] for $(5)^1\Sigma^+$ state are represented in Figs. 3 and 4, respectively, as vertical columns of points (in red).

The resulting IPA PECs of both states are listed in Table II and depicted, along with the "difference-based" PECs, in

TABLE II. Mass-invariant IPA potentials obtained for the $(5)^1\Sigma^+$ and $(3)^1\Pi$ states of the RbCs molecule. For the doubly degenerated $(3)^1\Pi$ state the IPA points correspond only to the "unperturbed" f component.

R (Å)	$U^{IPA}_{(5)^1\Sigma^+}$ (cm^{-1})	R (Å)	$U^{IPA}_{(3)^1\Pi}$ (cm^{-1})
4.1000	19807.379	4.0	18205.267
4.1732	19619.034	4.2	17857.830
4.2206	19475.817	4.4	17645.290
4.2751	19328.445	4.6	17514.442
4.3414	19169.777	4.8	17444.714
4.4250	18999.012	5.0	17419.908
4.5388	18817.032	5.2	17428.181
4.7395	18622.485	5.4	17460.458
4.9510	18562.362	5.6	17509.820
5.1866	18623.620	5.8	17570.475
5.4836	18815.085	6.0	17637.708
5.7135	18996.575	6.2	17706.632
5.9310	19165.930	6.4	17764.997
6.1447	19323.213	6.6	17791.839
6.3553	19470.917	6.8	17815.424
6.5625	19609.251	7.0	17831.022
6.7500	19720.086		

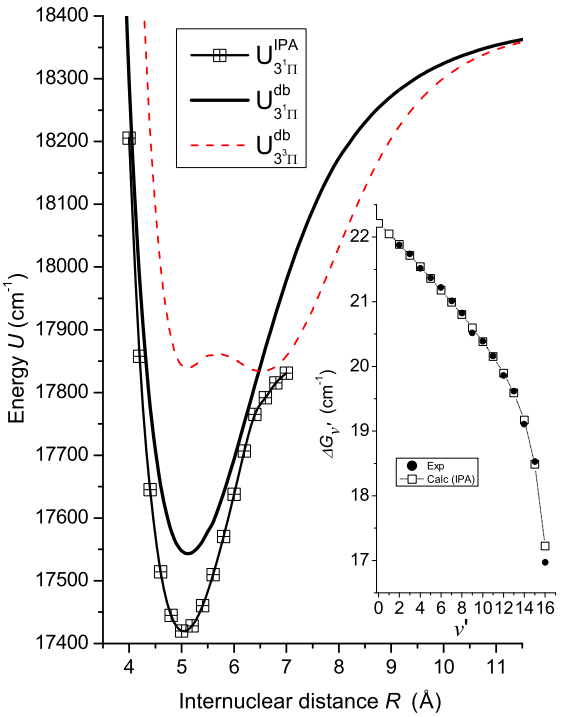

FIG. 5. Present empirical $U^{\rm IPA}$ and difference-based $U^{\rm db}$ adiabatic PECs constructed for $(3)^1\Pi$ and $(3)^3\Pi$ states. The inset displays the calculated and experimental [13] $\Delta G_{v'} = E_{v'+1} - E_{v'}$ values as a function of the vibrational quantum number v'.

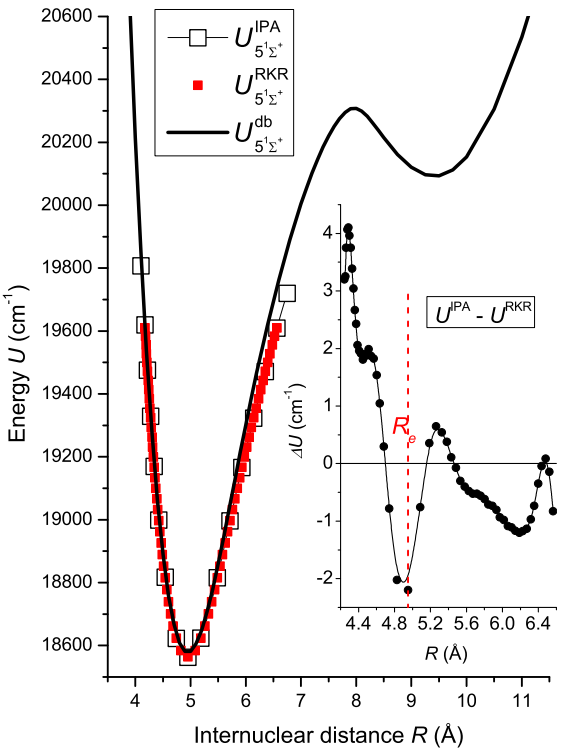

FIG. 6. Present empirical $U^{\rm IPA}$ and difference-based $U^{\rm db}$ adiabatic PECs constructed for the $(5)^1\Sigma^+$ state. The RKR potential from Ref. [14] is also presented. The inset represents the difference between the present IPA and RKR potentials.

TABLE III. Comparison of equilibrium distance R_e (in Å) and electronic energy T_e (in $\rm cm^{-1}$) available for the $(5)^1\Sigma^+$ and $(3)^1\Pi$ states of the RbCs molecule. The theoretical results correspond to pure Hund's (a) coupling case. The abbreviation PW marks the present work.

	$(5)^1\Sigma^+$		$(3)^1\Pi$	
Source	R_e	T_e	R_e	T_e
Theor. [17]	4.75	18902	5.04	17065
Theor. [31]	4.87	18562	5.06	17633
Theor. [32]	4.97	18481	5.24	17542
Theor. [22]	4.95	18551	5.07	17598
Theor. [PW]	4.95	18578	5.10	17542
Exps. [13,14]	4.951	18564.6		17418.9
Exp. [PW]	4.945	18562.33	5.041	17419.17

Fig. 5 and Fig. 6, respectively. The equilibrium parameters R_e and T_e of the present PECs are compared with the available literature data in Table III. One may note that the present R_e and T_e values are close enough to the preceding *ab initio* and empirical data for both states.

The present IPA potentials reproduce the observed term values with rms errors of 0.008 and 0.005 $\rm cm^{-1}$ for the $(3)^1\Pi$ and $(5)^1\Sigma^+$ states, respectively, in accordance with experimental spectroscopic accuracy. The residuals between observed and calculated term values can be seen in Figs. 7 and 8. More than 95% of the present FTS data obtained for the

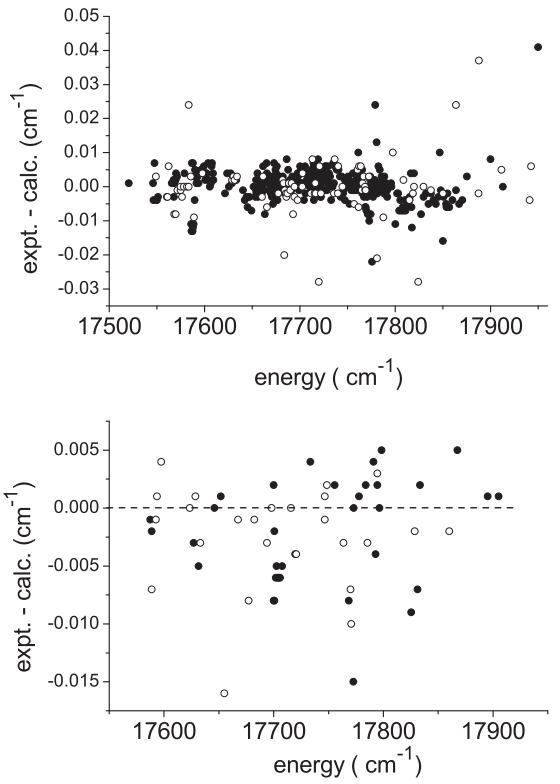

FIG. 7. Residuals $E^{\rm exp}$-$E^{\rm IPA}$ for $(3)^1\Pi$ state rovibronic levels observed in the present experiment. Empty circles denote e levels; full circles denote f levels. Upper layer, $^{85}Rb^{133}Cs$; lower layer, $^{87}Rb^{133}Cs$.

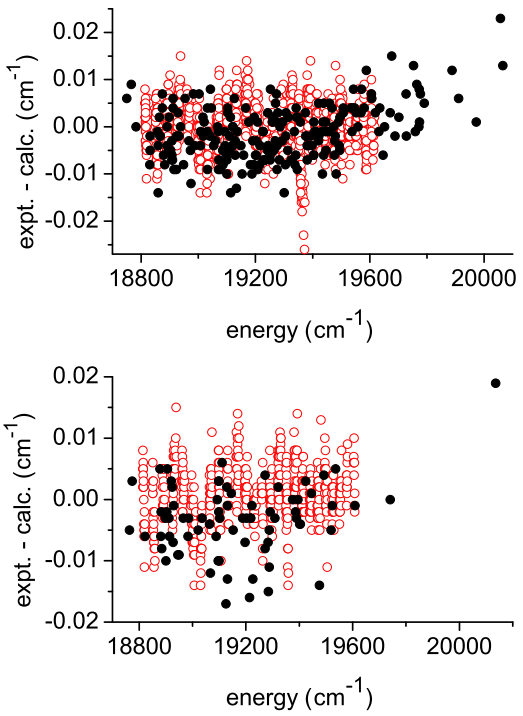

FIG. 8. Residuals $E^{\rm exp}$-$E^{\rm IPA}$ for the $(5)^1\Sigma^+$ state rovibronic levels included in the fit: black full circles, present experiment, red empty circles, data from Ref. [14]. Upper layer, $^{85}Rb^{133}Cs$; lower layer, $^{87}Rb^{133}Cs$.

$(3)^1\Pi$ state are reproduced within ± 0.01 cm^{-1}. It is interesting that for $^{87}Rb^{133}Cs$ (lower layer in Fig. 7) some slight systematic shift about -0.003 cm^{-1} can be observed. The residuals for the $(3)^1\Pi$ state term values from Ref. [13] are presented in the Supplemental Material [19]; they are substantially larger in accordance with those reported in Ref. [13] experimental inaccuracy of 0.1 cm^{-1}. The vibrational quanta of the $(3)^1\Pi$ state $\Delta G_{v'} = E_{v'+1} - E_{v'}$ abruptly decrease for $v' \geqslant 14$ levels (see the inset in Fig. 5) yielding a so-called shelf in the corresponding adiabatic PEC. Such a behavior can be attributed to avoided-crossing effect caused by the local spin-orbit coupling with the nearby triplet $(3)^3\Pi$ state.

The residuals for the $(5)^1\Sigma^+$ state also demonstrate high accuracy of the present IPA PEC which is, as expected, close to the preceding RKR potential from Ref. [14] (see the inset of Fig. 6). It should be mentioned, however, that the RKR PEC [14] reproduces the experimental term values with substantially less accuracy, especially outside of the observed range of small J' values; the corresponding figure is presented in the Supplemental Material [19]. It should be noted that the present FTS measurements significantly extend the range of experimental term values corresponding to high and intermediate rotational quantum numbers J' of both studied states. The range of observed vibrational levels was also expanded down to $v' = 0$ for the $(3)^1\Pi$ state and to $v' = 1$ for the $(5)^1\Sigma^+$ state.

B. The q factors of the $(3)^1\Pi$ state

For several levels of the double degenerated $(3)^1\Pi$ state the experimental term values of both e and f components were

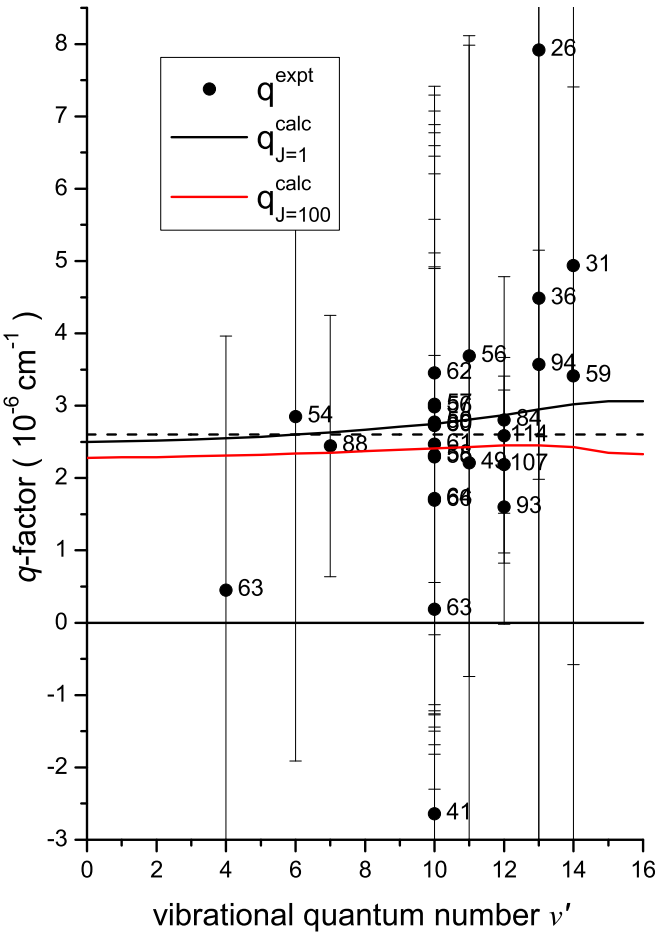

FIG. 9. Experimental and calculated q factors in the $(3)^1\Pi$ state of the $^{85}Rb^{133}Cs$ molecule. Rotational quantum number J' of measured levels is presented in the figure. Dashed horizontal line corresponds to the averaged experimental q value 2.6×10^{-6} cm^{-1}.

determined for the same v', J' levels and the corresponding $\Delta^{\rm exp}_{e/f}(v', J') = E^e_{^1\Pi} - E^f_{^1\Pi}$ splitting was obtained, see Fig. 9. In accordance with the second order perturbation theory, the observed e/f splitting can be approximated as

$$\Delta^{\rm exp}_{e/f} = q^{\rm exp}[J'(J'+1) - 1], \tag{8}$$

where the experimental $q^{\rm exp}$ factor is weakly dependent on v' and J' values. Because of great statistical errors of $q^{\rm exp}$ values v', J' dependence cannot be determined correctly from the present experiment. Averaging of all $q^{\rm exp}$ data yields value about 2.6×10^{-6} cm^{-1}.

In the case of a *regular* perturbation [33], the *ab initio* evaluated $Q(R)$ function (6) and the empirical parameter $s = 1.0455$ obtained during the present DPF analysis should be unambiguously related to the experimental q factors due to the approximate sum rules [34]

$$q^{\rm calc} \approx 2 \sum_{^1\Sigma^+} \sum_{v_{^1\Sigma^+}} \frac{|\langle v^{J'}_{^1\Pi} | BL_{^1\Pi-{}^1\Sigma^+} | v^{J'}_{^1\Sigma^+} \rangle|^2}{E^{J'}_{v_{^1\Pi}} - E^{J'}_{v_{^1\Sigma^+}}}$$
$$\approx s \langle v^{J'}_{^1\Pi} | BQB | v^{J'}_{^1\Pi} \rangle. \tag{9}$$

Indeed, Figure 9 demonstrates overall good agreement between the present measured $q^{\rm exp}$ and calculated $q^{\rm calc}$ values.

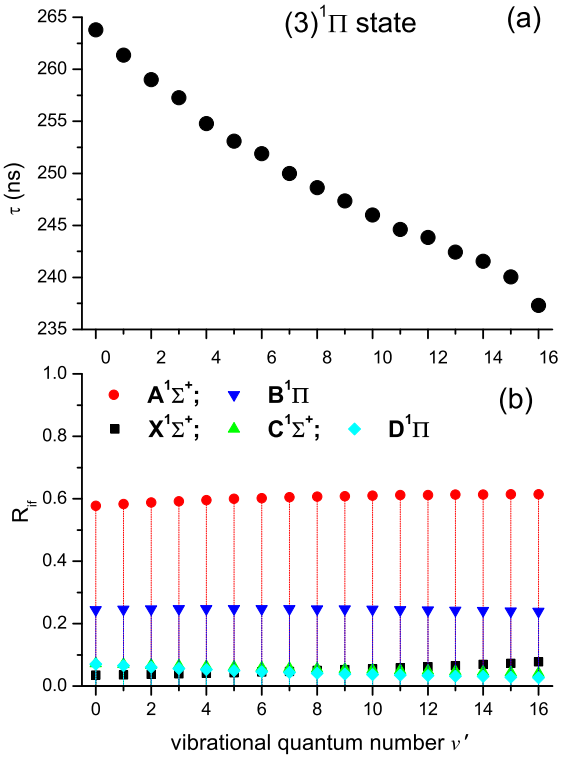

FIG. 10. Radiative lifetimes (a) and electronic branching ratios (b) of the $^{85}Rb^{133}Cs$ $(3)^1\Pi$ state as dependent on the vibrational quantum number evaluated according to the relations (10) and (11), respectively.

The value of the $(3)^1\Pi$ state q factor ($\approx 2.6 \times 10^{-6}$ cm^{-1}) appeared to be about 3 to 4 times larger than those estimated for the lower [35] $(2)^1\Pi$ and higher [22] $(4)^1\Pi$ lying states, namely $q_{(2)^1\Pi} \approx 5.9 \times 10^{-7}$ and $q_{(4)^1\Pi} \approx 8.0 \times 10^{-7}$ cm^{-1}. This difference could be attributed to the dominant contribution of the single $(4)^1\Sigma^+$ state into the sum (6). Furthermore, both relations (8) and (9) are valid only for low-lying vibrational levels of the $(3)^1\Pi$ state since the $Q(R)$ function has a singularity near the point $R \approx 4.2$ Å, where the repulsive walls of adiabatic $(3)^1\Pi$ and $(4)^1\Sigma^+$ PECs are crossing each other (see Fig. 1).

C. Radiative lifetimes and branching ratios of the $(3)^1\Pi$ and $(5)^1\Sigma^+$ states

The present *ab initio* adiabatic PECs $U_i^{ab}(R)$ and transition dipole moments $d_{ij}^{ab}(R)$, see Sec. V, were used to estimate a radiative lifetime τ_i of the upper $(3)^1\Pi$ and $(5)^1\Sigma^+$ states along with their vibronic branching ratios R_{if} into the lower-lying singlet state manifold. To avoid tedious summation over bound part and integration over continuum part of the vibrational spectra of the lower states we have used the approximate sum rule [34],

$$\frac{1}{\tau_i} \approx \frac{8\pi^2}{3\hbar\epsilon_0}\langle v_i^{J'}|\sum_j \left[\Delta U_{ij}^{ab}\right]^3\left[d_{ij}^{ab}\right]^2|v_i^{J'}\rangle, \quad (10)$$

$$R_{if} = \frac{\langle v_i^{J'}|\left[\Delta U_{if}^{ab}\right]^3\left[d_{if}^{ab}\right]^2|v_i^{J'}\rangle}{\langle v_i^{J'}|\sum_j \left[\Delta U_{ij}^{ab}\right]^3\left[d_{ij}^{ab}\right]^2|v_i^{J'}\rangle}, \quad (11)$$

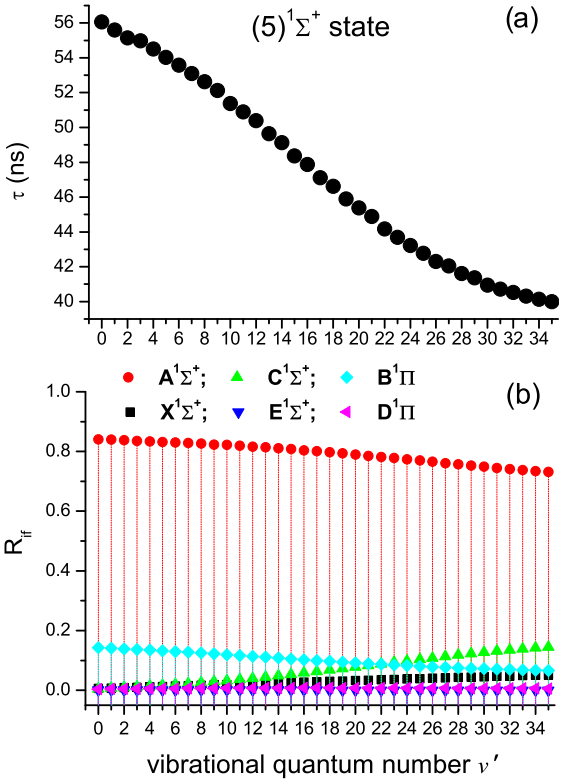

FIG. 11. Radiative lifetimes τ (a) and electronic branching ratios R_{if} (b) on the $^{85}Rb^{133}Cs$ $(5)^1\Sigma^+$ state as dependent of the vibrational quantum number evaluated according to the relations (10) and (11), respectively.

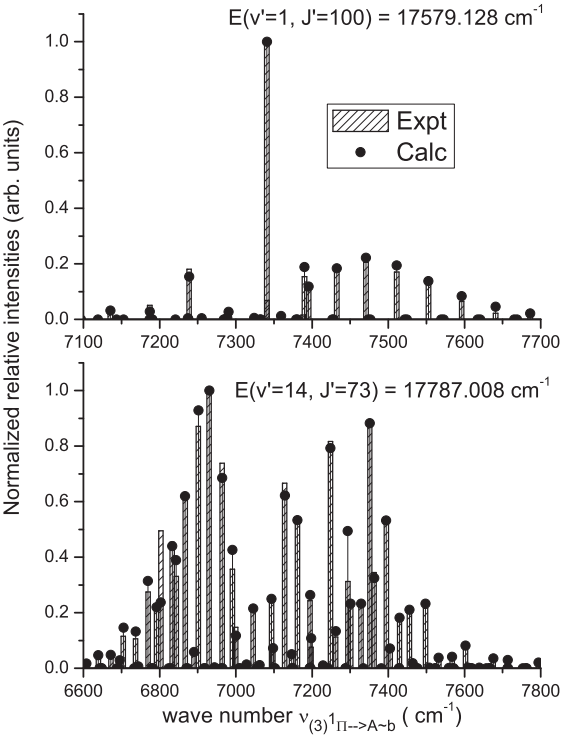

FIG. 12. Experimental I^{exp} and calculated I^{calc} relative intensity distributions in the singlet ($J' = J''$) LIF progressions with transitions from the particular $v' = 1$ (upper layer) and $v' = 14$ (lower layer) vibrational levels of the $(3)^1\Pi$ state to the lower-lying levels of the $A \sim b$ complex of the $^{85}Rb^{133}Cs$ isotopolog.

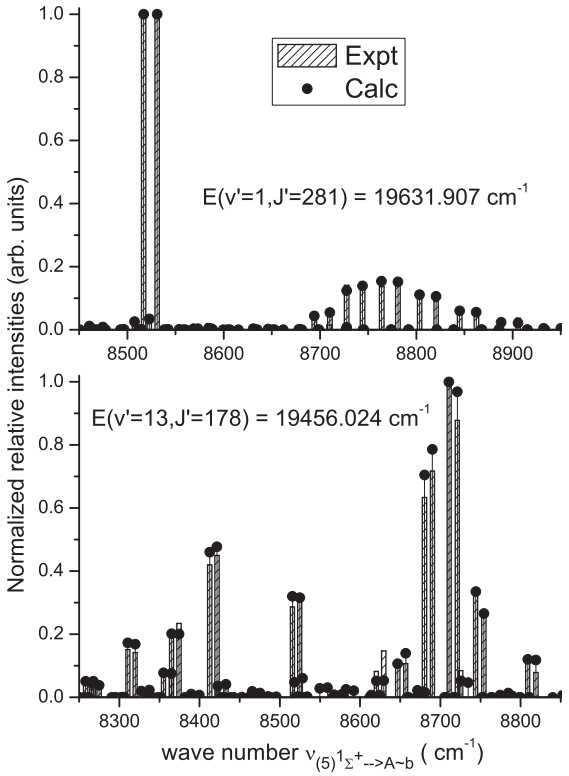

FIG. 13. The experimental $I^{\rm exp}$ and calculated $I^{\rm calc}$ relative intensity distribution in the doublet ($J'' = J' \pm 1$) LIF progressions from $v' = 1$ (upper layer) and $v' = 13$ (lower layer) vibrational levels of the $(5)^1\Sigma^+$ state to rovibronic levels of the $A \sim b$ complex of the $^{85}Rb^{133}Cs$ isotopolog.

where $\Delta U^{\rm ab}_{ij}(R) = U^{\rm ab}_i(R) - U^{\rm ab}_j(R)$ is the difference of the *ab initio* PECs, while the corresponding vibrational wave functions $|v_i^{J'}\rangle$ of the upper states were calculated using the present IPA potentials.

The resulting τ_i and R_{if} values for the $(3)^1\Pi$ and $(5)^1\Sigma^+$ states are depicted in Fig. 10 and Fig. 11, respectively. The calculated radiative lifetimes of both states rapidly decrease as the vibrational quantum number v' increases. The τ values predicted for the vibrational levels of the $(5)^1\Sigma^+$ state are about 5 to 6 times smaller than those for the rather long-living $(3)^1\Pi$ state.

According to the calculations, the dominant decay channel for both $i \in [(5)^1\Sigma^+; (3)^1\Pi]$ states is the optical transition to the lower $A^1\Sigma^+$ state (see Fig. 10 and Fig. 11) due to a large value of the relevant spin-allowed dipole moments (see the Supplemental Material [19]). The contribution of the $(5)^1\Sigma^+;(3)^1\Pi \rightarrow B^1\Pi$ transitions into the total decay does not exceed 30% while all other states (including the lowest ground state) contribute almost nothing. These estimates explain the fact that during the present LIF experiments we were not able to observe, except a few cases, very week $(3)^1\Pi \rightarrow X^1\Sigma^+$ and $(5)^1\Sigma^+ \rightarrow X^1\Sigma^+$ transitions hidden in the bush of strong $(4)^1\Sigma^+ \rightarrow X^1\Sigma^+$ progressions.

D. Intensity distributions in the $(3)^1\Pi \rightarrow A \sim b$ and $(5)^1\Sigma^+ \rightarrow A \sim b$ LIF progressions

The accuracy of the derived IPA potentials of both $(5)^1\Sigma^+$ and $(3)^1\Pi$ states as well as *ab initio* $(5)^1\Sigma^+ - A^1\Sigma^+$ and $(3)^1\Pi - A^1\Sigma^+$ transition dipole moments was additionally checked by a comparison of the simulated and measured relative intensity distributions in the particular $(3)^1\Pi \rightarrow A \sim b$ and $(5)^1\Sigma^+ \rightarrow A \sim b$ LIF progressions. The relevant rovibronic transition probabilities from the upper i state ($i \in (3)^1\Pi; (5)^1\Sigma^+$) to a lower-lying levels of the perturbed $A \sim b$ complex were calculated according to the relation

$$I^{\rm calc}_{i\rightarrow A\sim b} \sim \nu^4_{i\rightarrow A\sim b}\left|\langle v_i^{J'}\left|d^{\rm ab}_{i-A}\right|\phi_A^{J''}\rangle\right|^2,$$
$$\nu_{i\rightarrow A\sim b} = E^{J'}_{v_i'} - E^{J''}_{A\sim b}, \qquad (12)$$

where $\phi_A^{J''}(R)$ are the nonadiabatic vibrational wave functions belonging to the singlet component of the $A \sim b$ complex while $E^{J'}_{v_i'}$, $|v_i^{J'}\rangle$ are the adiabatic vibrational eigenvalues and eigenfunctions of the upper state calculated with the present IPA potentials. The comparison of the theoretical intensity distributions $I^{\rm calc}$ with their experimental counterparts $I^{\rm exp}$ is presented in Fig. 12 and Fig. 13. The observed and calculated intensities agree well enough, thus demonstrating the reliability of the performed analysis.

VII. CONCLUSIONS

We have demonstrated that the well-established perturbed levels of the singlet-triplet $A^1\Sigma^+ \sim b^3\Pi$ complex of the RbCs molecule can be successfully used for unambiguous rotational assignment of the high resolution FTS LIF progressions originating from the highly excited electronic states. The experimental rovibronic term values of the $(3)^1\Pi$ and $(5)^1\Sigma^+$ states were determined in a wide range of the rotational quantum number J'. The range of observed vibrational levels was expanded down to $v' = 0$ for the $(3)^1\Pi$ state and $v' = 1$ for the $(5)^1\Sigma^+$ state. The obtained data were involved, together with the preceding term values [13,14], in a direct-potential-fit analysis performed in the framework of the inverted perturbation approach. The simulated intensity distributions in the observed LIF progressions are found to be remarkably close to their experimental counterparts. A good agreement between the experimental and calculated q factors validates the *unique perturber* approximation [33] for the $(3)^1\Pi$ state. Based on the *ab initio* transition dipole moments estimate of lifetimes and vibronic branching ratios confirms a dominant contribution of the $(5)^1\Sigma^+ \rightarrow A^1\Sigma^+$ and $(3)^1\Pi \rightarrow A^1\Sigma^+$ transitions into total radiative decay of the both upper states.

ACKNOWLEDGMENTS

The Moscow team is grateful for the support from RFBR Grant No. 16-03-00529a. The Riga team acknowledges support from the University of Latvia (Base/Performance No. A5-AZ27 and No. Y9-B013) and support from the EU project Laserlab-Europe H2020 EC-GA654148.

[1] K. Bergmann, N. V. Vitanov, and B. W. Shore, J. Chem. Phys. **142**, 170901 (2015).

[2] E. A. Pazyuk, A. V. Zaitsevskii, A. V. Stolyarov, M. Tamanis, and R. Ferber, Russ. Chem. Rev. **84**, 1001 (2015).

[3] J. Tennyson, J. Chem. Phys. **145**, 120901 (2016).
[4] T. Takekoshi, L. Reichsöllner, A. Schindewolf, J. M. Hutson, C. R. Le Sueur, O. Dulieu, F. Ferlaino, R. Grimm, and H.-Ch. Nägerl, Phys. Rev. Lett. **113**, 205301 (2014).
[5] P. K. Molony, P. D. Gregory, Z. Ji, B. Lu, M. P. Köppinger, C. R. L. Sueur, C. L. Blackley, J. M. Hutson, and S. L. Cornish, Phys. Rev. Lett. **113**, 255301 (2014).
[6] C. D. Bruzewicz, M. Gustavsson, T. Shimasaki, and D. DeMille, New J. Phys. **16**, 023018 (2014).
[7] T. Shimasaki, J.-T. Kim, and D. DeMille, Chem. Phys. Chem. **17**, 1 (2016).
[8] G. Quéméner and P. S. Julienne, Chem. Rev. **112**, 4949 (2012).
[9] A. F. Nogueira, C. E. Fellows, and T. Bergeman, J. Chem. Phys. **129**, 136101 (2008).
[10] V. Zuters, O. Docenko, M. Tamanis, R. Ferber, V. V. Meshkov, E. A. Pazyuk, and A. V. Stolyarov, Phys. Rev. A **87**, 022504 (2013).
[11] T. Gustavsson, C. Amiot, and J. Verges, Mol. Phys. **64**, 293 (1988).
[12] B. Kim and K. Yoshihara, Chem. Phys. Lett. **212**, 271 (1993).
[13] B. Kim and K. Yoshihara, J. Chem. Phys. **100**, 1849 (1994).
[14] Y. Yoon, Y. Lee, T. Kim, J. S. Ahn, Y. Jung, B. Kim, and S. Lee, J. Chem. Phys. **114**, 8926 (2001).
[15] Y. Lee, Y. Yoon, S. Lee, and B. Kim, J. Phys. Chem. A **113**, 12187 (2009).
[16] A. Kruzins, K. Alps, O. Docenko, I. Klincare, M. Tamanis, R. Ferber, E. A. Pazyuk, and A. V. Stolyarov, J. Chem. Phys. **141**, 184309 (2014).
[17] A. R. Allouche, M. Korek, K. Fakherddin, A. Chaalan, M. Dagher, F. Taher, and M. Aubert-Frecon, J. Phys. B **33**, 2307 (2000).
[18] T. Bergeman, C. E. Fellows, R. F. Gutterres, and C. Amiot, Phys. Rev. A **67**, 050501 (2003).
[19] See Supplemental Material at http://link.aps.org/supplemental/10.1103/PhysRevA.96.022510 for *ab initio L*-coupling matrix elements, difference based potentials and electronic transition dipole moments, measured and fitted term values and their comparison with previous data, calculated term values of A $\sim$ b complex.
[20] A. Pashov, W. Jastrzebski, and P. Kowalczyk, Comput. Phys. Commun. **128**, 622 (2000).
[21] H.-J. Werner, P. J. Knowles, R. Lindh, F. R. Manby, M. Schutz, P. Celani, T. Korona, G. Rauhut, R. D. Amos, A. Bernhardsson, A. Berning, D. L. Cooper, M. J. O. Deegan, A. J. Dobbyn, F. Eckert, C. Hampel, G. Hetzer, A. W. Lloyd, S. J. McNicholas, W. Meyer, M. E. Mura, A. Nicklass, P. Palmieri, U. Schumann, H. Stoll, A. J. Stone, R. Tarroni, and T. Thosteinsson, MOLPRO, Version 2010.1, a package of *ab initio* programs.
[22] A. Zaitsevskii, E. A. Pazyuk, A. V. Stolyarov, O. Docenko, I. Klincare, O. Nikolayeva, M. Auzinsh, M. Tamanis, and R. Ferber, Phys. Rev. A **71**, 012510 (2005).
[23] O. Docenko, M. Tamanis, R. Ferber, H. Knöckel, and E. Tiemann, Phys. Rev. A **83**, 052519 (2011).
[24] E. A. Pazyuk, E. I. Revina, and A. V. Stolyarov, Chem. Phys. **462**, 51 (2015).
[25] R. B. Ross, J. M. Powers, T. Atashroo, W. C. Ermler, L. A. LaJohn, and P. A. Christiansen, J. Chem. Phys. **93**, 6654 (1990).
[26] J. Werner and P. J. Knowles, J. Chem. Phys. **82**, 5053 (1985).
[27] P. J. Knowles and H.-J. Werner, Theor. Chim. Acta **84**, 95 (1992).
[28] P. Fuentealba, H. Stoll, L. V. Szentpaly, P. Schwerdtfeger, and H. Preuss, J. Phys. B **16**, L323 (1983).
[29] NIST Atomic data base [http://physics.nist.gov/].
[30] J. Mitroy, M. S. Safronova, and C. W. Clark, J. Phys. B **43**, 202001 (2010).
[31] D. Pavolini, T. Gustavsson, F. Spiegelmann, and J.-P. Daudey, J. Phys. B **22**, 1721 (1989).
[32] I. S. Lim, W. C. Lee, Y. S. Lee, and G.-H. Jeung, J. Chem. Phys. **124**, 234307 (2006).
[33] R. W. Field and H. Lefebvre-Brion, *The Spectra and Dynamics of Diatomic Molecules* (Elsevier, Amsterdam, 2004).
[34] E. A. Pazyuk, A. V. Stolyarov, and V. I. Pupyshev, Chem. Phys. Lett. **228**, 219 (1994).
[35] T. Gustavsson, C. Amiot, and J. Verges, Chem. Phys. Lett. **143**, 101 (1988).